

Experimental study on plasma-catalytic synthesis of hydrocarbons from syngas

Di Li, Vandad-Julien Rohani, Frédéric Fabry, Aravind Parakkulam Ramaswamy, Mohamed Sennour, Laurent Fulcheri

▶ **To cite this version:**

Di Li, Vandad-Julien Rohani, Frédéric Fabry, Aravind Parakkulam Ramaswamy, Mohamed Sennour, et al.. Experimental study on plasma-catalytic synthesis of hydrocarbons from syngas. Applied Catalysis A : General, 2019, 588, pp.117269. 10.1016/j.apcata.2019.117269 . hal-02459265

HAL Id: hal-02459265

https://minesparis-psl.hal.science/hal-02459265

Submitted on 21 Dec 2021

HAL is a multi-disciplinary open access archive for the deposit and dissemination of scientific research documents, whether they are published or not. The documents may come from teaching and research institutions in France or abroad, or from public or private research centers.

L'archive ouverte pluridisciplinaire **HAL**, est destinée au dépôt et à la diffusion de documents scientifiques de niveau recherche, publiés ou non, émanant des établissements d'enseignement et de recherche français ou étrangers, des laboratoires publics ou privés.



Distributed under a Creative Commons Attribution - NonCommercial 4.0 International License

Version of Record: https://www.sciencedirect.com/science/article/pii/S0926860X19304247
Manuscript_34e89a472a0a2a985abfd3f6560ac846

Experimental study on plasma-catalytic synthesis of hydrocarbons from syngas

Di Li[a,*], *Vandad Rohani*[a], *Frédéric Fabry*[a], *Aravind Parakkulam Ramaswamy*[a], *Mohamed Sennour*[b], *Laurent Fulcheri*[a]

[a]PSL Research University, MINES ParisTech, PERSEE - Centre Procédés, Énergies renouvelables et Systèmes énergétiques 1 Rue Claude Daunesse, 06904 Sophia Antipolis, France

[b]PSL Research University, MINES ParisTech, Centre des Matériaux, 63-65 rue Henri Auguste Desbruères - B.P. 87, 91003 Evry Cedex, France

Corresponding Author

*E-mail: di.li@mines-paristech.fr

Highlights

A series of ambient drying cobalt/silica aerogel catalysts were prepared, characterized, and applied for plasma driven FTS under ambient conditions.

C1-C5 hydrocarbons and liquid oxygenates were synthesized under ambient conditions with a relative low SIE.

The catalyst samples exhibited enhancement on the conversions of reactants and the formation of liquid oxygenates.

© 2019 published by Elsevier. This manuscript is made available under the CC BY NC user license
https://creativecommons.org/licenses/by-nc/4.0/

ABSTRACT: This paper is dedicated to the experimental study of FTS synthesis via a non-thermal plasma-catalytic pathway under ambient conditions. In our study, a vertical tubular DBD reactor containing packed catalysts was established with its analytical apparatus. Different Co/SiO_2 aerogel catalysts were synthesized by ambient drying method and then characterized. The variable studies were conducted without packing, and then the performance of the catalysts was evaluated. The results indicate that a considerable concentration of C1 to C5 hydrocarbons were synthesized at ambient conditions with relatively low specific input energies (below 18 kJ/L). Moreover, the Co/SiO_2 aerogel catalysts can promote not only the synthesis of C2-C5 hydrocarbons rather than CH_4 and CO_2 but also the formation of liquid organic oxides. The possible reaction pathways of the non-thermal plasma promoted FTS associated with catalysis were proposed. The work demonstrates a new approach of FTS and broadens the field of further improvement on FTS.

KEYWORDS: Hydrocarbon synthesis, Non-thermal plasma, Ambient conditions, Fischer-Tropsch, Catalysts

1. INTRODUCTION

Nowadays, global warming due to the continuous accumulation of greenhouse gases in the atmosphere has been one of the most critical issues in human society. Meanwhile, the demand for fossil fuels, especially petroleum, continues to increase. Within this context, the synthetic hydrocarbons and hydrocarbon oxides produced from biomass, natural gas, biogases and wastes through BTL (Biomass To Liquids) or GTL (Gas To Liquids) processes have drawn great interests due to the great potential for CO_2 cycling and low carbon emission in industries in recent years. These processes can be described as transforming feedstock (biomass or CO_2 with CH_4) to intermediates (normally syngas) by gasification or dry reforming and synthesizing liquid fuels and useful chemicals by Fischer-Tropsch synthesis (FTS). As one of the key techniques, FTS was first proposed and published by two German chemists[1], is one of the most critical technologies for these processes. The main reaction of FTS can be briefly described as:

$$2(n+1)H_2 + \mathrm{n}CO \xrightarrow{\text{catalysts}} C_nH_{2n+2} + nH_2O$$

A functional catalyst is necessary for FTS process as its significant effects on the distribution of the final products and the ability to lower the energy barrier of the main reaction. All metals of Group VIII and some other alkali metals such as copper, zinc, and rhenium have a noticeable catalytic activity for F-T synthesis reactions[2]. Cobalt and iron are the most popular metals in FTS catalysts according to their high activity, stability, and selectivity. Although Co is more expensive than Fe, it is almost three times more active in the view of site basis than Fe according to chemisorption analysis[3] and shows higher resistance to oxidation by water and lower activity to Water Gas Shift Reaction[4].

Another crucial aspect of the research concerning of the FTS catalyst is the supports. Silica, alumina, and titanium oxide are the most common supports for Co catalysts. Silica-supported cobalt catalysts exhibit a high catalytic activity and liquid hydrocarbon selectivity in FTS due to the physical and chemical properties: 1) high surface area which makes high Co dispersion at relatively high loadings of Co [5, 6]; 2) controllable wide range of pore size which ensures a uniform diffusion of gas components; and 3) adjustable surface chemistry property which enables a high reducibility of metal [7]. Li and co-workers[8, 9] have investigated the catalytic performance of Co loaded MCM-41, SBA-15, and SiO_2 with different pore size. Results indicated that the mesoporous structure Co/SiO_2 has a moderate cobalt particle size and the highest dispersion, which contributes to high CO hydrogenation activity and coincides with Saib's work [10]. Dunn and co-workers[11-14] demonstrated that the mesoporous silica aerogel supported nanocrystal Co catalysts were remarkably active to FTS with high selectivity for the C10+ hydrocarbons. Meanwhile, some studies[10] have also revealed that the surface hydroxyl group on the surface of silica formed by the preparation process could lead to the formation of irreducible cobalt hydroxide. However, the modification of the hydrophobic surface property is possible for a silica aerogel support via introducing hydrophobic groups [15, 16].

Although FTS has been considered as a developed and promising technique, some drawbacks are still difficult to overcome: the demand for high pressure (~several tens of bars) and heating (~150-300°C). Plasma, which is a group of ionized gas that can be generated by many methods such as electric discharges, combustion, and flames, offers a unique pathway to induce chemical reactions, unlike thermo-chemical pathway due to its high concentration of energetic and chemically active species [17]. Non-thermal plasmas, which are far from

thermodynamic equilibrium, can be generated at ambient temperature and pressure with a low power requirement. The combination of plasma and catalysts described as plasma-catalysis, which has been widely considered as a promising method for organic synthesis, is a complicated and vague process in a one-stage system, where the catalyst is introduced in the discharge zone directly. The synergistic effects between plasma and catalysts can modify both the chemical and physical properties of each other [18-20]. On the one hand, plasma might restructure the catalysts and the surface of supports to promote chemical adsorption and reaction and the catalysts with supports, in turn, might enhance the plasma phenomenon [21-23]. On the other hand, the dramatic reduction of discharge volume could alter, even impair the discharge behavior, therefore decreasing the power of plasma [22, 24]. Until now, plasma-catalysis has been explored, studied, and applied on some chemical processes such as nitrogen fixation and more importantly, CO_2 reforming and gasification [25, 26]. The successful combination of plasma with FTS can achieve an overall plasma induced GTL or BTL process, where the plasma discharge can be easily generated by applying voltage. Moreover, as renewable energy shares higher and higher proportion in electricity generation, this plasma induced process offers a new perspective for utilizing, storing renewable energy and achieving low carbon emissions in industries.

However, only few efforts have dedicated to the study on plasma promoted hydrocarbon synthesis via FTS. Our group [27, 28] has conducted some experiments on FTS via very high-pressure plasma without catalysts; the results indicated that even at very high pressure (~2 MP) with high specific input energy (varying from 1000 to 10000 kJ/mol), light hydrocarbons are dominant among all the products. The absence of catalysts may be the reason for the low selectivity to C_{5+} paraffin and olefins. Meanwhile, Al-Harrasi et al. [29] have studied plasma promoted FTS with external heating and operating pressure and w35% (w/w) Cu/Co=1 (weight ratio) alloy loaded aluminosilicate (Al_2SiO_5) ceramic foam monolith. The results have shown the existence of C_{5+} at a low H_2/Co ratio (~0.5) with specific input energy of 2500 kJ/mol. Until now, no research on non-thermal plasma promoted FTS at ambient conditions is found.

Under this context, this study aims to explore the possibility of hydrocarbons synthesis from syngas via plasma-catalytic promoted FTS at ambient conditions. The plasma experiments were firstly conducted in a tubular dielectric barrier discharge reactor at ambient pressure and

temperature, and the influence of different variables like total flow rate and a different ratio of H_2 and CO were investigated. The hydrophobic SiO_2 aerogel was synthesized as the support for Co catalyst due to its hydrophobicity and high porosity, which could avoid the extreme reduction of discharge volume. The Co loaded hydrophobic SiO_2 aerogel catalysts (Co/SiO_2) were designed, synthesized by different methods and Co precursors, and then dried at ambient conditions. Finally, the catalysts were calcined, placed into the reactor, and the catalytic performance of the catalysts was investigated and presented. This study offers a new perspective of hydrocarbon synthesis at ambient pressure and temperature via plasma promoted FTS associated with catalysis.

2. EXPERIMENTAL

2.1. Experimental setup

The schematic diagram of the experimental setup for plasma experiments is shown in Figure 1. The setup mainly consisted of three parts: a power supply system, a reaction system, and a products collection and analysis system. The schematic diagram and photo of the DBD reactor are presented in Figure S2. The reactor included a borosilicate dielectric tube with an inner and outer diameter of 10 and 12 mm, an inner high voltage electrode, an outer grounded electrode, and two movable caps. The inner high-voltage electrode was an aluminum rod with a diameter of 6 mm installed coaxially with the dielectric tube. The two movable Teflon caps (6 mm i.d. × 10 mm o.d.) with 12 semi-circle pores (1mm i.d.) evenly distributed around were coupled with the aluminum rod to ensure the concentricity of the electrode and ceramic tube. The grounded electrode was stainless-steel coils with a length of 200 mm rolled surrounding the borosilicate tube. Therefore, the discharge volume and the catalytic zone was calculated as 10.1 cm^3. A compressed air ejector was coaxially installed under the reactor to avoid the possible overheating issue of the reactor and the outer electrode. Before the reactor, the flow rate of the inlet gas was controlled by two flowmeters (Brooks Sho-Rate Models 1355G, calibrated by massive flowmeter) respectively. In this work, the total flow rate was fixed at 30 mL_n/min.

The power supply system, applied to the reactor, is composed of a signal function generator (HP 33120A), an audio amplifier (IMG Stageline STA-1400) and a transformer. The amplifying output level range of the audio amplifier varies from “-80 dB” to “0 dB”, therefore the peak-to-

peak voltage can be adjusted. Different signals with a variable frequency were generated through the function generator. In this work, the frequency and the peak-to-peak voltage of the sinusoidal signal were fixed at 3 kHz and 6 kV respectively. The Lissajous method, which was firstly introduced by Manley in 1943[30] was applied to calculate the discharge power via connecting a capacitor (3.9 nF) in series with the reactor. Two high-voltage probes were applied to measure the voltage of the plasma reactor and the capacitor; two temperature probes were installed right in the gas inlet and outlet of the reactor respectively to measure the temperature of the inlet and outlet gas; one pressure probe was installed before the gas inlet to monitor the pressure of inlet gas. The real-time data of temperature and pressure were monitored and recorded simultaneously on a computer via a Keysight 34970A Data Acquisition unit. The electrical data were monitored via a digital oscilloscope (HP Hewlett Packard 54615B) in real-time and recorded by the computer separately. The data files were recorded by 1000 points for each of 2 channels (one for the reactor and the other one for capacitor) once with time.

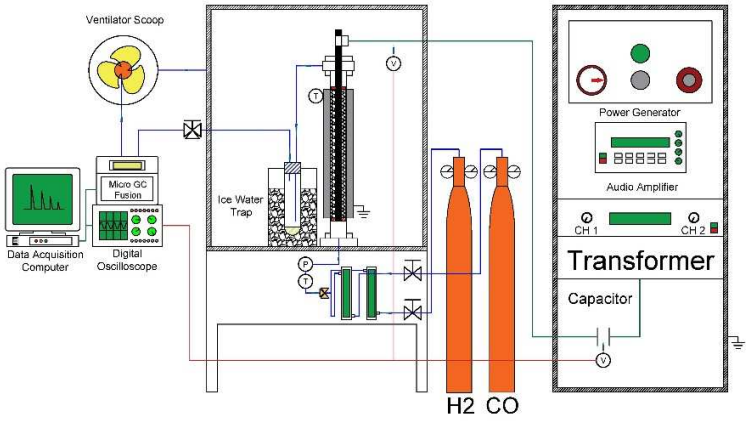


Figure 1. Schematic diagram of the experimental setup

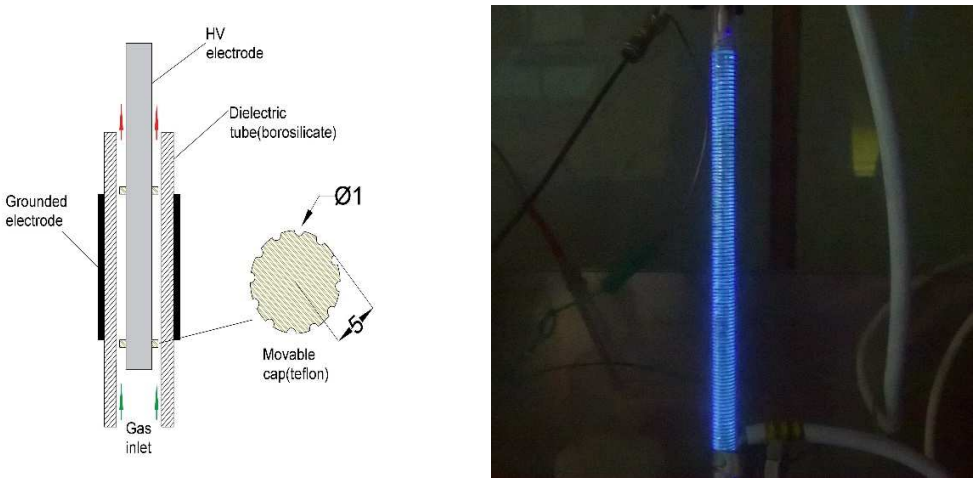


Figure 2. Photo and schematic diagram of the DBD reactor

2.2. Preparation of catalysts

A series of Co/SiO_2 aerogel catalysts with a various targeted mass ratio of Co to SiO_2 aerogel were firstly prepared via the sol-gel method. The aiming amount of $CoCl_2 \cdot 6H_2O$ and $Co(NO_3)_2 \cdot 6H_2O$ (Acros Organics, ≥ 99%) was dissolved in 15.0 g of ethanol (Fisher Scientific, Absolute) in a polyethylene vial while stirring. Simultaneously, 10.0 g of polyethoxydisiloxane (P75W20, PCAS, <30%) was added to the ethanolic solution and stirred for 5 mins. After that, 2625 μL of distilled water was added to the mixed solution, and 2955 μL (3-Aminopropyl) triethoxysilane (APTES, Thermo Fisher, 98%) solution (APTES: Ethanol = 1:50) was added to adjust the pH value for gelation. The final mixture solution was covered and allowed to gel and age at 60 °C for 48 h. Nevertheless, we found that the sample synthesized by the nitrate precursor cannot form homogeneous gels. Following the aging, 35 mL of hexamethyldisilazane (HMDZ, Acros Organics, 98%) was added to the gels synthesized by the chloride precursor and remained covered for 3 nights at ambient conditions to remove the hydroxyl groups. Following hydrophobizing, the hydrophobic silica gels were washed in ethanol for 5 times (in 2 days) to remove excessive HMDZ. The gels were transferred into an oven and dried for 2h at 140 °C. The final gels were first calcined in air at 400 °C for 5h with a heating rate of 10 °C/min to obtain Cobalt-silica aerogels. These series of catalysts were named as 10 or 20Cl-S (the number 10 or 20 represents the percentage of loading amount, Cl refers to $CoCl_2$ precursor, and S refers to the sol-gel method).

Another series of Co/SiO_2 aerogel catalysts with the same targeted mass ratio as which were prepared via the sol-gel method were prepared by the wetness impregnation method. The targeted ethanolic solution of $CoCl_2 \cdot 6H_2O$ and $Co(NO_3)_2 \cdot 6H_2O$ (Acros Organics, ≥99%) were introduced into the same volume of 0 wt% SiO_2 aerogels prepared by the sol-gel method and impregnated for one night. Following the impregnation procedure, the samples were dried, calcined, and reduced as the same procedures as those prepared by the sol-gel method. These series of catalysts were named as 20Cl-I or 20NO-I (Cl and NO refer to $CoCl_2$ and $Co(NO_3)_2$ precursors, and I represents the impregnation method). Before the experiments, the catalysts samples were reduced in H_2/N_2 (5%/95%) flow at 600 °C for 10 h with a heating rate of 10 °C/min.

2.3. Experimental analysis

The gaseous products were analyzed online by a micro gas chromatography (Micro GC Fusion) equipped with two channels (an Rt-Molsieve 5 Å R0.25mm, L 10m column and an Rt-Q-Bond R0.25mm, L12m column) and two thermal conductivity detectors (TCD). An icy water trap was used to condense the liquid products before the micro GC. The liquid products were analyzed offline using a gas chromatography-mass spectrometer (GCMS-QP2010, Shimadzu). The difference of the gas volume before and after the discharge was measured at the outlet by a soap-film flowmeter. The plasma experiments were repeated three times. The experimental uncertainties (E) of ±10% for GC and 12% for GC-MS were mainly contributed by the calibration ($E_{calibration}$) and sample measurements ($E_{repeatance}$).

$E = E_{calibration} + E_{repeatance} \approx 10\%$ (for GC), 12% (for GC-MS)

According to the measurements of GC before and during each experiment, the conversion(x) is calculated as:

$$x_{H_2} = \frac{moles\ of\ H_2\ comsumed}{moles\ of\ H_2\ inlet}\ \% \quad (1)$$

$$x_{CO} = \frac{moles\ of\ CO\ comsumed}{moles\ of\ CO\ inlet}\ \% \quad (2)$$

$$x_{total} = \frac{\sum moles\ of\ reactants\ comsumed}{\sum moles\ of\ reactants\ inlet}\ \% \quad (3)$$

The selectivity of gaseous products can be calculated as:

$$S_{CO_2} = \frac{moles\ of\ CO_2\ produced}{moles\ of\ CO\ consumed} \times 100\ \% \quad (4)$$

$$S_{C_xH_y} = \frac{x \times moles\ of\ C_xH_y\ produced}{moles\ of\ CO\ consumed} \times 100\ \% \quad (5)$$

Then the total selectivity of liquid products can be calculated due to:

$$S_{liquid} = 100\% - S_{CO_2} - S_{C_xH_y} \quad (6)$$

The specific input energy (SIE) is defined as the formula following:

$$SIE = \frac{Plasma\ power(kW)}{Flow\ rate(\frac{L}{min})} * 60(\frac{s}{min}) \quad (7)$$

The energy efficiency of the reactor based on the gas conversion is defined as the gas converted per unit of discharge power:

$$E_{CO} = \frac{x_{CO}}{power\ of\ discharge} \times 100(\%/W) \quad (8)$$

$$E_{H_2} = \frac{x_{H_2}}{power\ of\ discharge} \times 100(\%/W) \quad (9)$$

The carbon balance (CB) is calculated as:

$$CB = \frac{CO_{out} + CO_{2\ out} + xC_xH_{y\ out}}{CO_{in}} \quad (10)$$

3. RESULTS AND DISCUSSION

3.1. Catalyst characterization

Table 1 illustrates the specific surface area, pore volume, and average pore size of these series of catalyst samples. The results revealed that all the samples were a mesoporous structure with negligible or inexistence of micropores. Compared to the silica aerogel, the surface area and pore volume of Co loaded samples was lower since the cobalt compounds could block the smaller nanopore structure, which results in the decrease in pore volume and surface area. It was found that even 20% of Co loading amount did not obviously decrease the surface area and pore volume, indicating the mesoporous structure was well retained.

Table 1. Surface area and porous properties of the catalyst samples

Catalysts	surface area[a] (m^2/g)	pore volume[b] (cm^3/g)	average pore diameter[b] (nm)	t-plot micropore area[c] (m^2/g)
aerogels	736	1.72	8.2	20.79
10Cl-S	719	1.31	6.0	26.87
20Cl-S	708	1.27	7.9	28.96
20NO-I	624	1.19	7.9	/
20Cl-I	655	1.22	8.1	/

[a] Brunauer-Emmett-Teller method.

[b] Barrett-Joyner-Halenda method determination via N_2 adsorption data.

[c] t-plot method via Harkins-Jura equation.

The XRD patterns of these series of catalysts are presented in Figure 3. It was found that the peaks of crystalline cobalt phases were barely observed among these samples. The reason of this phenomenon could be the high dispersion of cobalt species (particularly among the samples prepared by the sol-gel method), which attributes to nanosized clusters of cobalt species inside the mesopores or on the surface, leads to evading detection by XRD[31]. Moreover, the formation of a strong interaction between cobalt and SiO_2 can also result in this phenomenon[32].

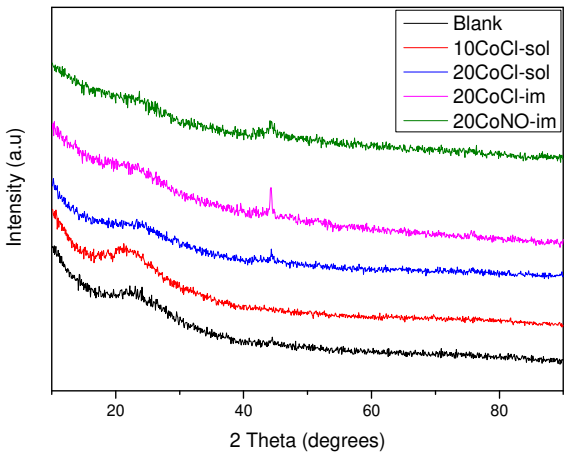


Figure 3. The XRD patterns of the Co/SiO_2 aerogel samples

The Co 2p XPS spectra of aerogel and the samples prepared by the sol-gel method are shown in Figure 4. The curves were smoothed with the Gaussian method by Avantage 6.0. As the half-peak width of Co2p3 is more than 3 eV, implying the existence of superposition of several peaks, different kinds of cobalt species exist in the supports.

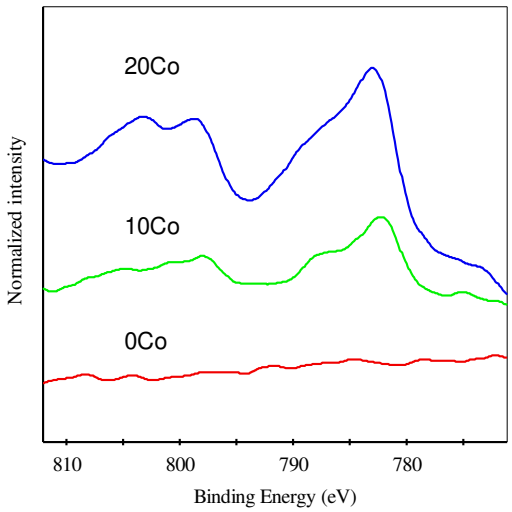


Figure 4. The Co 2p XPS spectra of aerogel, 10Cl-S, and 20 Cl-S samples.

The further fitted peaking results of the 20Cl-S sample are shown in Figure 5. Three Co species are known to exist in the 777–815 eV region: CoO, Co_2O_3, and Co_3O_4 [33, 34]. Since the BE of Co^{3+} is uncharacteristically lower than that of Co^{2+} attributed to final state (relaxation) effect, and some researchers reported that the Co2p lines of Co^{2+} when Co is deposited onto other oxides such as Si, Mo and Ti followed by oxidation, shift to higher BE up to 781.7 eV[35]. The main oxidized peak was considered as $Co^{2+,}$ and the unobvious peak was referred to Co_3O_4 [33, 34]. Further study was essential to identify the oxidized cobalt peaks of high binding energy. Despite the difference in the intensity of the peaks, the peaking results of the samples prepared by the impregnation method are similar to the samples prepared via the sol-gel method.

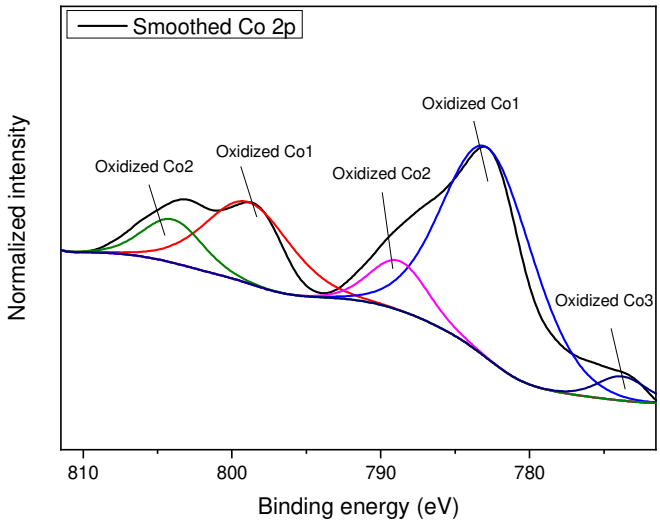


Figure 5. XPS peaking in the Co 2p region of the 20Cl-S sample

The micrographs of these Co/SiO_2 aerogel catalysts are illustrated in Figure 6. The matrix of silica aerogel is easily observed, which is comprised of many visible clusters of spherical clusters. Meanwhile, a small number of cobalt particles are also found in figure (1). Notably, in figure (2) a fibrous or filamentous structure is found as a different phase from SiO_2 spherical clusters. According to Matsuzaki's and Jiménez's research [33, 36], it has been reported that one part of the cobalt phase in aerogels can connect with -O- during the hydrolytic and polycondensation and form -O-Co-O- bridge and the chain structure. This interaction between cobalt catalysts with the support finally leads to an inactivate unreducible structure [37]. Few filamentous structures were observed in the micrographs of the samples prepared by the impregnation method, indicating that the bridge structure of the cobalt phase with the bone structure of the silica aerogel was barely formed via the impregnation method.

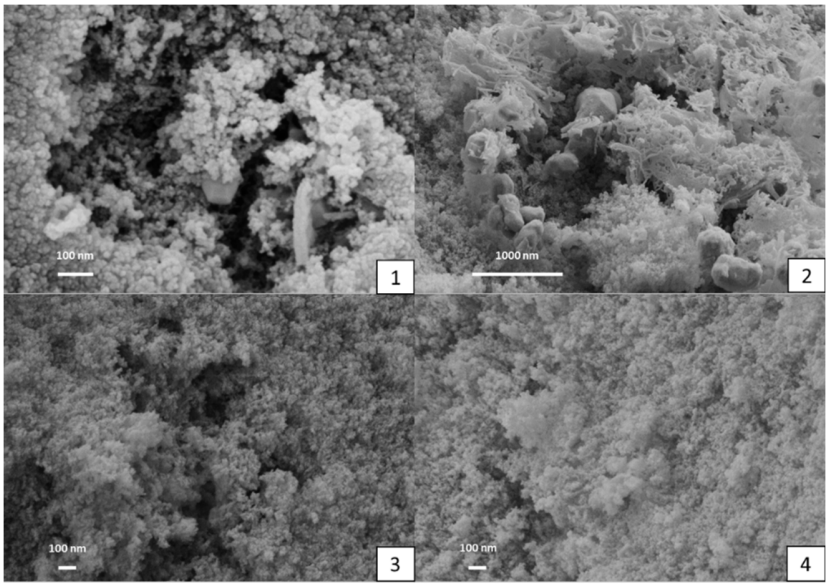


Figure 6. The SEM micrographs of: (1) 10Cl-S, (2) 20Cl-S, (3) 20Cl-I, (4) 20NO-I

Later the HRTEM bright field images and selected area diffraction applied to confirm the CoO_2 structure as shown in Figure 7 and Figure 8. The results reveal that the particle was a hexagonal crystallite in space group P-3m1 with a lattice parameter of a=2.82 Å, b=2.82Å, c= 4.24Å, which is confirmed to be CoO_2 structure[38]. As calcining cobalt precursors in the air could hardly form the unstable CoO_2, the speculation of the existence pf CoO_2–Si structure is reasonable. On the contrary to CoO_2, which is highly reducible, the CoO_2–Si structure exhibits low reducibility and low catalytic activity according to the mentioned publications[33, 36, 38]. Based on the results, the Co species in the SiO_2 aerogel support is confirmed to be catalytically active CoO and Co_3O_4 catalytically inactive CoO_2-Si formed by the strong interaction between catalyst and support due to the difficulties on reduction.

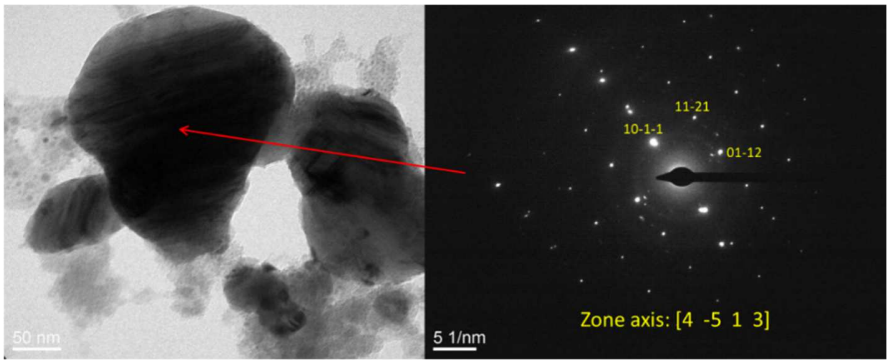


Figure 7. The HRTEM bright field images and selected area diffraction of 20Cl-S sample

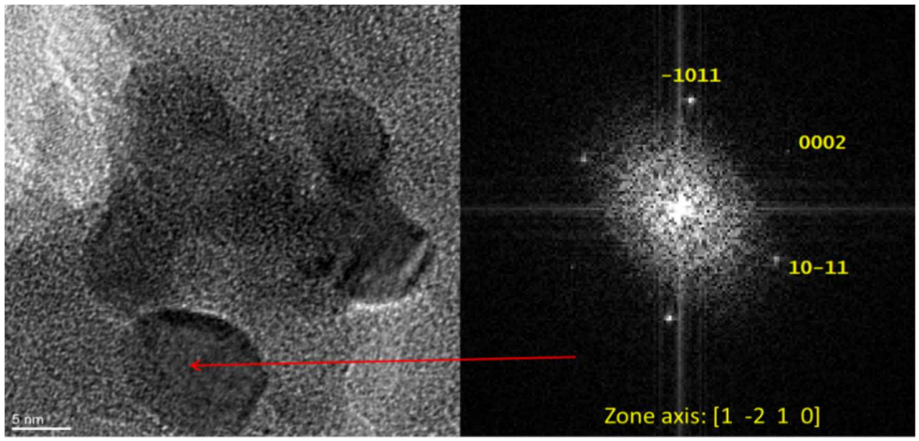


Figure 8. The HRTEM bright field images and selected area diffraction of 20NO-I sample

3.2. Total flow rate

The first experiments were conducted under different total flowrate. The liquid products were collected for 90 mins and then dissolved by 3 mL of pure acetone. Due to the negligible liquid produced via these tests, only the results of the gas products were listed. The measurements were repeated three times (at 30 min, 60 min, and 90 min) after the discharge behavior was stable. The SIE, conversions of CO and H_2 varying by total flow rate are shown in Figure 9. Table 2 and Table 3 represents the analysis of gaseous products analysis, the energy efficiency of the reactants, and carbon balance and the concentration of C2-C5 hydrocarbon species in the product gas varying by total flow rate, respectively. H_2 to CO ratio of these the tests was fixed at 1:1.

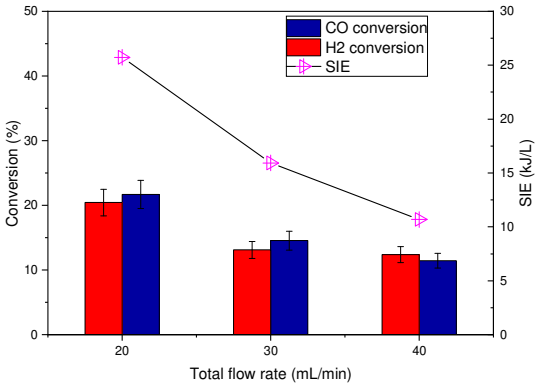


Figure 9. The SIE and conversions as a function of total flow rate (H_2 to CO=1:1, frequency: 3000 Hz, peak-to-peak voltage: 6 kV)

Table 2. Gaseous products analysis of the experiments varying by total flow rate (H_2 to CO=1:1, frequency: 3000 Hz, peak-to-peak voltage: 6 kV)

Total flow rate	Selectivity			Energy efficiency(%/W)		Carbon balance
	CO_2	CH_4	C2-C5	H_2	CO	
40 mLn/min	0.51	0.23	0.10	1.74	1.61	0.981
30 mLn/min	0.57	0.31	0.11	1.65	1.83	0.985
20 mLn/min	0.50	0.27	0.09	2.38	2.53	0.951

Table 3. Concentration distribution of C2-C5 hydrocarbons in the product gas varying by total flow rate[2]

Total flow rate	C_2H_6 (ppm)	C_2H_2+C_2H_4 (ppm)	C_3H_8 (ppm)	C3[1] (ppm)	C_4H_{10} (ppm)	C4[1] (ppm)	C5[1] (ppm)
40 mLn/min	1921	67	520	401	74	67	37
30 mLn/min	2583	64	550	420	68	175	49
20 mLn/min	3278	71	634	515	79	215	56

[1] Referring to Cn species excluding n-paraffin.

[2] The experimental uncertainty is ±10%.

It is quite interesting that C2-C5 hydrocarbon species, which were hardly detected in the previous work of our group via high-pressure plasma [27, 28], were found among the yield of the products with a relatively low SIE. A high selectivity has been The CO disproportioning reaction has been well comprehended that the vibrational excitation could significantly accelerate it under non-thermal plasma [39]:

$$CO + CO \rightarrow CO_2 + C,\ E_a = 6\ eV/mol$$

The activation energy of the disproportioning reaction is much less than the energy of direct CO bond dissociation (11.2 eV). This explains the high concentration of CO_2 among the gaseous products. The increase of the CO portion in the feeding gases increased the selectivity to CO_2 as the CO disproportioning reaction was promoted. As a result, the carbon balance was lower and more carbon deposits were formed. Similar to the initial reactions of FTS, methane, and acetylene can be synthesized from syngas in non-thermal plasma conditions [40]:

$$CO + 3H_2 \rightarrow CH_4 + H_2O$$

$$2CO + 3H_2 \rightarrow C_2H_2 + 2H_2O$$

Logically, a lower flow rate induces a longer residence time, thus resulting in higher SIE as reactant molecules spend more time in the discharge, and vice versa. Consequently, the conversions and the concentrations of long-chain products were higher at a lower flow rate. According to the results, the conversions of reactants and the carbon balance were similar when varying the total flow rate from 40 mL_n/min to 30 mL_n/min, while significantly changed under a total flow rate of 20 mL_n/min under similar discharge power. The carbon balance under a total flow rate of 20 mL_n/min was notably lower than the other tests and the selectivity towards C2-5 was slightly lower, implying the more fraction of carbon from CO finally formed carbon deposits due to CO disproportioning reaction. While within a range of total flow rate higher than 20 mL_n/min, fewer carbon deposits were formed. Therefore, a low flow rate naturally led to higher SIE, thus increasing conversions of reactants, but the carbon deposition was also more dramatic, leading to a lower total selectivity towards hydrocarbons.

3.3. H_2 to CO ratio

Taking account of the carbon balance, conversions, and the convenience of flowrate control of gas components, a total flowrate of 30 mL_n/min was chosen for these series of tests. Figure 10 illustrates the SIE and conversions as a function of different H_2 to CO ratio. The results listed in Table 4 demonstrate the gaseous products analysis, the energy efficiency of the reactants, and carbon balance. Table 5 demonstrates the concentration of C2-C5 hydrocarbon species in the product gas.

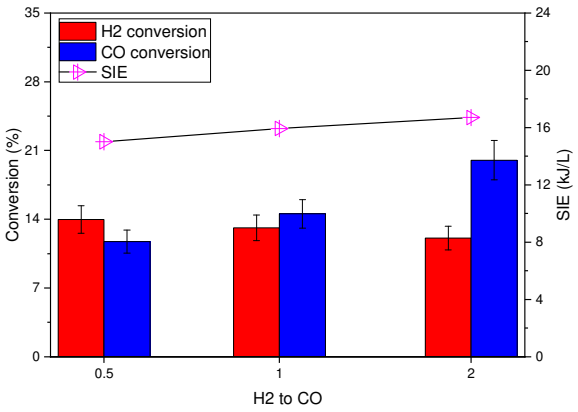


Figure 10. The SIE and conversions as a function of different H_2 to CO ratio (total flow rate: 30 mL_n/min, frequency: 3000 Hz, peak-to-peak voltage: 6 kV)

Table 4. Gaseous products analysis of the experiments varying by different H_2 to CO ratio (total flow rate: 30 mL_n/min, frequency: 3000 Hz, peak-to-peak voltage: 6 kV)

H_2 to CO ratio	Selectivity			Energy efficiency(%/W)		Carbon balance
	CO_2	CH_4	C2-C5	H_2	CO	
0.5	0.59	0.29	0.10	1.86	1.56	0.969
1	0.57	0.31	0.11	1.65	1.83	0.985
2	0.48	0.36	0.13	1.45	2.41	0.989

Table 5. Concentration distribution of C2-C5 hydrocarbons in the product gas varying by different H_2 to CO ratio[2]

H_2 to CO ratio	C_2H_6 (ppm)	C_2H_2+C_2H_4 (ppm)	C_3H_8 (ppm)	C3[1] (ppm)	C_4H_{10} (ppm)	C4[1] (ppm)	C5[1] (ppm)
0.5	2270	106	490	350	72	195	82
1	2583	64	550	420	68	175	49
2	2425	46	496	347	61	148	37

[1] Referring to Cn species excluding n-paraffin.

[2] The experimental uncertainty is ±10%.

It was found that the ratio of H_2/CO significantly affected the conversions, selectivity, and distribution of different gaseous species. As the dissociation energy (4.52 eV) and relative

breakdown voltage of H_2 are lower than those of CO (~11.16 eV), a high proportion of H_2 significantly enhanced the conversion of CO up to 20.1%, synthesizing hydrocarbons rather than CO_2. It should also be noticed that the conversion of H_2 decreased with the increase of H_2 in the feed gases due to its extremely fast deexcitation. As the discharge atmosphere was more enriched activated H^+ species due to its lower dissociation energy, more saturated hydrocarbons were formed instead of unsaturated species even under the condition of a high proportion of CO. Moreover, it was found that increasing the proportion of H_2 of the gas components sufficiently increased the carbon balance and decreased the selectivity to CO_2 in the gaseous products. Considering the FTS mechanism and the results, we deem that the exited H^+ species can activate and react CO molecules by ion-molecular reactions, thus promoting the conversion of CO and synthesizing hydrocarbons rather than CO_2 when increasing H_2 proportion. Meanwhile, a part of carbon produced from CO disproportioning reaction can react with exited H species to participate in chain initiation and growth reactions in the reactor, leading to the improvement on carbon balance from 0.969 to 0.989:

$$C^* + 2H^* \rightarrow CH_2^*$$

$$nCH_2^* \rightarrow C_nH_{2n}^*$$

Where * refers to an excited state.

Therefore, similar to conventional FTS, which is normally manipulated under an H_2/CO ratio of 2:1 or even higher, a high H_2 proportion in gas component significantly promotes the conversion the conversions of CO and improves the carbon balance with less formation of CO_2 within a certain range. Considering the total conversions and carbon deposition, an H_2/CO ratio of 2:1 was chosen for further experiments.

3.4. Catalytic performance

According to previous tests without catalysts, the H_2 to CO ratio of was fixed at 2 to evaluate the catalytical performance for the further experiments. The catalysts samples were reduced in the H_2/N_2 (5%/95%) flow at 600 °C for 10 h with a heating rate of 10 °C/min before placing into the reactor.

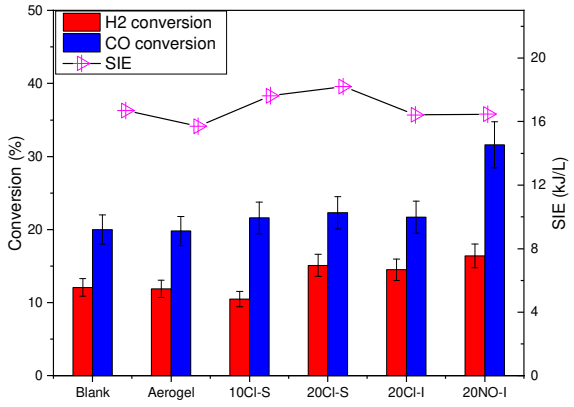


Figure 11. The SIE and conversions varying by the different catalysts (total flow rate: 30 mL_n/min, frequency: 3000 Hz, peak-to-peak voltage: 6 kV)

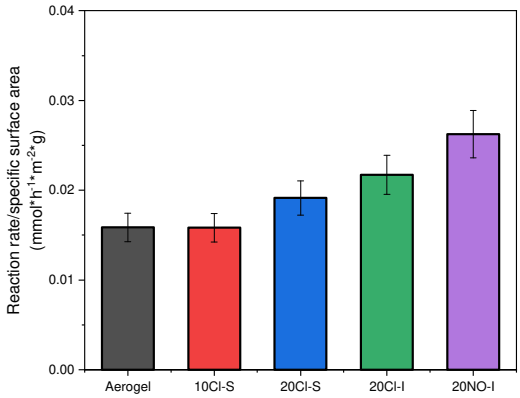


Figure 12. The reaction rates normalized to specific surface area varying by the different catalysts (total flow rate: 30 mL_n/min, frequency: 3000 Hz, peak-to-peak voltage: 6 kV)

Figure 11 shows the SIE, conversions varying by the different catalysts; Figure 12 illustrates the reaction rates normalized to specific surface area varying by the different catalysts. Comparing the results of tests with and without SiO_2 aerogels, the SIE of the test with aerogels was slightly lower, while the introduction of Co/SiO_2 increased the SIE. The explanation could be that on the one hand, the introduction of aerogels reduced the discharge volume in the reactor, leading to lower absorbed power; on the other hand, the conductive property of the discharge space was modified and also the discharge behavior could be altered in turn, particularly with cobalt, leading to an increase of the discharge power. Meanwhile, as the dispersion of cobalt was not uniform via the impregnation method, the excessive cobalt caused more collapses and blocking of the pore structure as illustrated in the supplementary data, which caused the decrease of SIE. The conversions of the reactants, particularly CO, was remarkably high after placing the

catalyst sample 20NO-I into the reactor. However, the other catalyst samples prepared by the chloride precursors did not obviously exhibit promoting the conversions even the Cl-S samples had a better dispersion of Co. One explanation could be that chloride ion was well-known harmful for FTS; the residual chloride ion in the catalysts could prohibit the conversion of reactants.

Table 6. Gaseous products analysis of the experiments varying by the different catalysts (total flow rate: 30 mL_n/min, H_2 to CO ratio = 2:1, peak-to-peak voltage: 6 kV, frequency: 3 kHz)

Catalysts	Selectivity				Energy efficiency(%/W)		Carbon balance
	CO_2	CH_4	C2-C5	Liquid products	H_2	CO	
Blank	0.48	0.36	0.12	/	1.45	2.41	0.989
Aerogel	0.60	0.29	0.09	0.03	1.52	2.52	0.999
10Cl-S	0.53	0.28	0.12	0.07	1.45	2.41	1.06
20Cl-S	0.46	0.28	0.13	0.13	1.65	2.45	0.993
20Cl-I	0.53	0.28	0.10	0.09	1.76	2.64	0.982
20NO-I	0.44	0.27	0.12	0.17	1.98	3.83	0.946

Table 7. Concentration distribution of C2-C5 hydrocarbons in the product gas varying by the different catalysts[2]

Catalysts	C_2H_6 (ppm)	C_2H_2+C_2H_4 (ppm)	C_3H_8 (ppm)	C3[1] (ppm)	C_4H_{10} (ppm)	C4[1] (ppm)	C5[1] (ppm)
Aerogel	1916	45	524	277	73	111	31
10Cl-S	2303	46	594	346	126	141	59
20Cl-S	3232	59	865	296	208	148	92
20Cl-I	2600	49	562	372	90	106	37
20NO-I	4608	66	856	667	163	124	51

[1] Referring to Cn species excluding n-paraffin.

[2] The experimental uncertainty is ±10%.

Table 8. Liquid product yield analysis of the experiments varying by the different catalysts by GC-MS(total flow rate: 30 mL_n/min, H_2 to CO ratio = 2:1, peak-to-peak voltage: 6 kV, frequency: 3 kHz)[1]

Catalysts	H_2O (%)	CH_3OH (%)	CH_3CHO (%)	CH_3CH_2OH (%)
10CoCl-sol	93.0	6.1	0.58	0.28
20CoCl-sol	92.6	6.2	0.74	0.26
20CoCl-im	93.1	6.1	0.62	trace
20CoNO-im	85.0	13.4	1.3	0.32

[1] The experimental uncertainty is ±12%

The gaseous products analysis and the concentrations of C2-C5 gaseous products formed after plasma treatments with different catalyst samples are presented in Table 6 and Table 7, respectively. Table 8 demonstrates the liquid product analysis of the experiments varying by the different catalysts. Packing SiO_2 aerogel led to the decrease of the selectivity to hydrocarbons mainly due to the decrease of SIE and discharge volume. Moreover, the selectivity to CO_2 was remarkably enhanced probably due to plasma-surface interaction such as the change of residence time of active species on the surface, local hot spots, and enhancement of the local electric field. Compared with aerogels, all the samples with cobalt remarkably promoted the formation of liquid products. Givotov et al. have reported the direct synthesis of formaldehyde and then conversion into methanol via non-thermal plasma processing of syngas with sufficient high SIE [17]:

$$CO + H_2 \rightarrow CH_2O$$

$$H_2 + CH_2O \rightarrow CH_3OH$$

However, it has been proved that CH_2O radicals are easily to decompose under plasma discharge [17], thus resulting in a low selectivity towards liquid chemicals without packing. While with packing, a part of methanol, ethanol, and acetaldehyde, which is attractive as these organic oxides are essential chemicals, was detected among the liquid products. Besides, the sample 20Cl-S and 20NO-I also promoted the formation of long-chain hydrocarbon products rather than CH_4 and slightly decreased the selectivity to CO_2. The increase of Co loading amount from 10% to 20% significantly benefit the formation of liquid products and C2-C5 hydrocarbons.

Thus, the cobalt catalysts were confirmed to promote the hydrocarbon synthesis and decrease the energy barrier of the formation of oxides such as alcohols and aldehydes with higher energy efficiency in our reactor. The explanations can be, on the one hand, the strong sorption behavior of the mesoporous structure in the support could inhibit the decomposition of CH_2O radicals as mircodishcarge is difficult to form in mesopores under typical DBD plasma (Derby sheath > mesopores). On the other hand, the introduction of Co catalysts promoted the conversions of reactants and the formation of CH_2O radicals. In the previous section, we found even the cobalt in the samples prepared by the sol-gel method was better dispersed, while a part of Co species could partially connect with SiO_2 bone structure to form inactive Co species. This explained the higher activity of 20NO-I than 20Cl-S as shown in Figure 12. It should be noted that the reaction rates in Figure 12 were normalized to the specific surface area of the catalysts as the origin of active sites of catalysts was not well identified yet. Meanwhile, the plasma-catalytic surface reactions could be affected by packing any solid supports or catalysts. Therefore, the results indicated that the catalytic performance of the samples prepared by nitrate precursor was better than the others with a higher concentration of C2-C5 hydrocarbons, organic oxides, and particularly higher energy efficiency. One point should be noticed that a part of water component could be produced via FTS reactions; however, the condensed vapor from the air could also be notable due to the temperature difference between the icy water trap and the atmosphere.

The catalysts after the experiments were also characterized by XPS. Except that a very small peak of carbon was detected, no significant change was found in the surveys. No apparent phenomena of deactivation were found until 90 mins among all the tests with the catalysts. The C1s peak region of some samples smoothed by Gaussian method is shown in Figure 13. The carbon species found in the blank sample was more like carbon deposition (C-C bonding at 284.5 eV). While among the Co loaded samples, less carbon and different carbon species were found. The XPS peaking of the 20CoCl-sol sample after the plasma experiments was illustrated in Figure 14. Not only carbon deposition (C-C bonding at 284.5 eV) but also organic carbon species (C-O bonding at 286 eV, O-C=O at 288 eV, unobtrusive satellite peak at 291 eV) were detected as the fitting peaks in Figure 14. Moreover, a notable π-π^* satellite peak occurred at around 295.5 eV of binding energy without peaking. According to Gardella's and Beamson's study [41, 42], the extended delocalized electrons of the aromatic ring in ethylene terephthalate or pentaphenyl-trimethyl-siloxane structure results in the significantly high binding energy of π-

π^* satellite peak. Generally, it was not necessary to form a polymer, but the monomers could also lead to this phenomenon. Considering the obvious organic O-C=O and C-O peaks, the result implies the existence of C5+ organics on the catalysts.

Consequently, besides the organic oxides such as alcohols and aldehydes, a small part of esters and C5+ organics were synthesized on the catalysts. Due to their high boiling point and low production, these organics were beyond determination by GC-MS after condensation. The result confirms that the cobalt catalysts promoted the formation of organics and hydrocarbons via plasma catalytic approach. Therefore, less carbon deposition but more organic carbons were detected. The result supports that cobalt catalysts can promote the reactions of the exited C species with H, leading to the formation of hydrocarbons rather than CO_2.

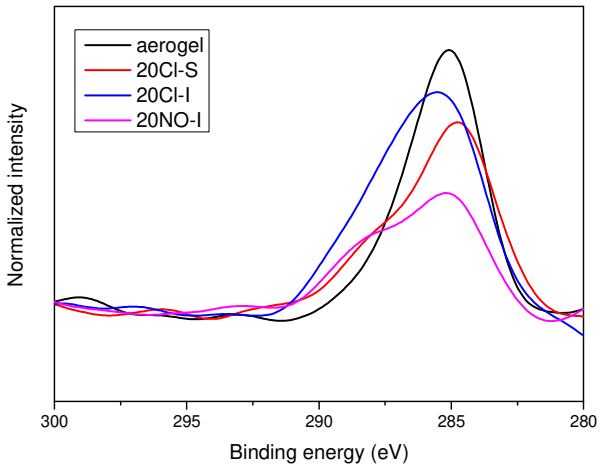


Figure 13. XPS peak region in C1s of the corresponding catalysts after the plasma experiments (smoothed by Gaussian method): Aerogel, 20Cl-S, 20Cl-I, 20NO-I

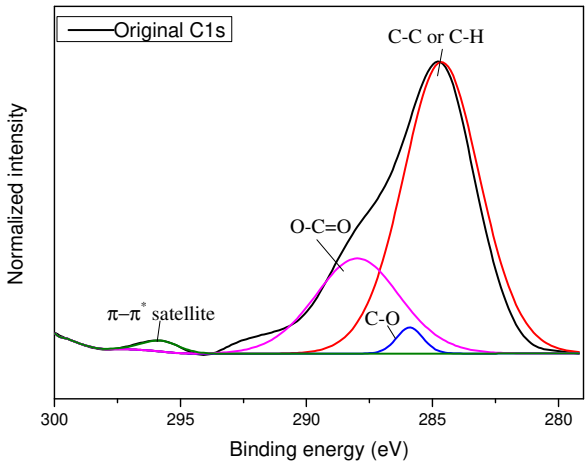


Figure 14. XPS peaking region in C1s of the 20CoCl-sol sample after the plasma experiments

To compare our work with other plasma FTS and conventional FTS process, we defined a total energy efficiency based on the conversion of reactants to the energy consumed by the process as:

$$EE_{total} = \frac{moles\ of\ reactants\ consumed}{energy\ consumed} (\text{mmol/kJ})$$

Figure 15 shows the total energy efficiency as a function of conversion of reactants by comparing this work with the plasma FTS of Vandad's and Iwarere's works and conventional FTS of Im-orb's work [43]. Noted that as the total conversion of Vandad's and Iwarere's works was overall less than 1%, we overestimated the value of 1%. Moreover, since the size of the reactor in this work was nearly four times than the reactor of their works, the nominal total conversion was estimated at 4% for the comparison. Obviously, much higher conversions can be achieved with relatively higher energy efficiency in our work comparing to Vandad's and Iwarere's works, where a very high SIE was applied in the reactor even ignoring the energy used for compressing inlet gas. More importantly, only CH_4, C2, and C3 species with very low concentrations were detected in their works. While not only CH_4 and C2-C5 hydrocarbons, but also some useful liquid chemicals such as methanol in liquid products and aromatics in aerogels were detected with much higher concentration. Comparing to a typical industrial FTS process, the overall energy efficiency of plasma process was much lower than a typical industrial FTS process as the industrial FTS process includes recycling, gas turbine power generating and heat recovery, leading to very high conversion and low energy consumption. However, the research

of plasma FTS process is on the very beginning stage and has great potential of improvement for the further studies.

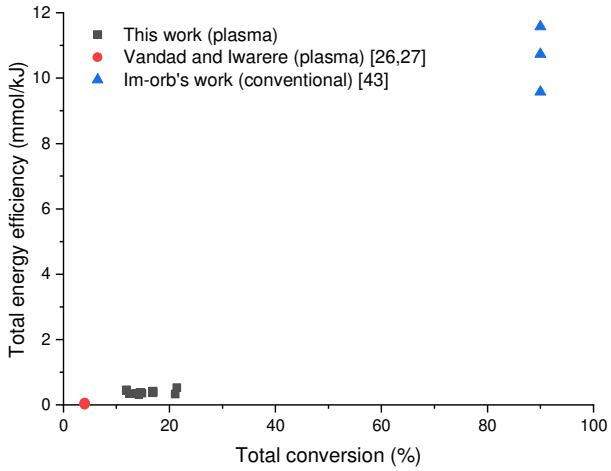


Figure 15. Experimental data collected from the literature for plasma and conventional FTS process, showing total energy efficiency as a function of conversion of reactants.

To summarize, the cobalt catalyst played a vital role in the plasma promoted FTS as it significantly enhanced the conversions and promoted the higher hydrocarbon synthesis and the formation of organic oxides.

4. CONCLUSION

This work aimed to explore the possibility of the non-thermal plasma promoted FTS at ambient conditions. For this purpose, an experimental bench was realized. Different cobalt loaded silica aerogel catalysts were designed, synthesized at ambient conditions after surface modification and then characterized. After that, plasma experiments without/with catalysts were conducted.

C1 to C5 hydrocarbons were synthesized by this way at ambient conditions with a relatively low energy consumption compared to existing work in which the external pressure, heating, and high SIE were essential. The introduction of the cobalt catalysts significantly enhanced the

synthesis of liquid organics and C2-C5 hydrocarbons rather than CO_2 and CH_4 from syngas by a plasma catalysis approach. Moreover, methanol, ethanol, and acetaldehyde were synthesized and detected among the liquid products via the catalysts; a small part of esters and C5+ organics were detected on the catalysts. 20NO-I catalyst sample demonstrated a notable catalytic performance with remarkably high energy efficiency.

Then, a parametric experimental study revealed that a large portion of H_2 in the feeding gas favored the conversion of CO and the formation of hydrocarbons. A low flow rate naturally led to higher SIE, thus increasing conversions of reactants. However, the over selectivity towards hydrocarbons was lower due to the higher proportion of carbon deposits. It was also found that introducing aerogel support slightly decreased the discharge power as we expected. Nevertheless, the increase of Co loading amount significantly increases the yield of hydrocarbons and organic oxides but does not necessarily increase the discharge power due to the block and collapse of the porous structure.

In conclusion, the non-thermal plasma pathway provides a new perspective of FTS process at ambient conditions with relatively low energy consumption and broaden the field of further improvements.

ACKNOWLEDGMENT

This research was carried out in the frame of the cooperative doctoral programs (ParisTech/CSC) supported by the China Scholarship Council (CSC). The authors warmly acknowledge CSC for their support.

ABBREVIATIONS

FTS, Fischer-Tropsch Synthesis; BTL, Biomass To Liquids; GTL Gas To Liquids; DBD, dielectric barrier discharge; XRD, X-ray diffraction; XPS, X-ray photoelectron spectroscopy; SEM, scanning electron microscope; TEM, Transmission electron microscope; Q, charge; U, voltage; R resistance; C, capacitance; L, inductance; HV, high voltage; GC, gas chromatography; Rt-Molsieve, fused silica PLOT column; Rt-Q-Bond, fused silica PLOT column; TCD, thermal conductivity detector; P75W20, polyethoxydisiloxane; APTES, (3-Aminopropyl)

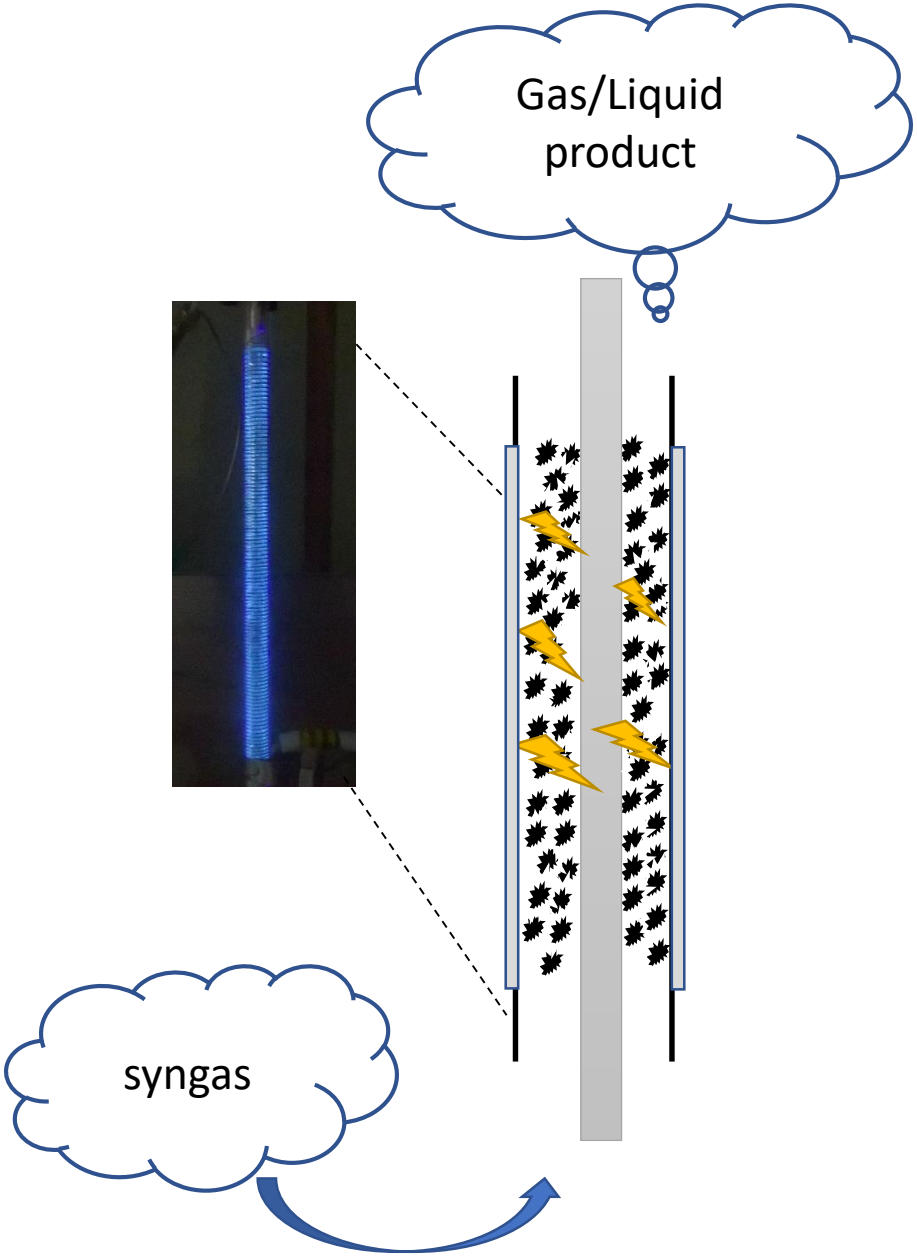
triethoxysilane; HMDZ, hexamethyldisilazane; BE, binding energy; E_a, activation energy; SIE, specific energy input; C1-5, hydrocarbon molecular including 1 to 5 carbon atoms.

REFERENCES

[1] F. Fischer, H. Tropsch, The synthesis of petroleum at atmospheric pressures from gasification products of coal, Brennstoff-Chemie, 7 (1926) 97-104.
[2] M. Vannice, The catalytic synthesis of hydrocarbons from H2CO mixtures over the group VIII metals: I. The specific activities and product distributions of supported metals, Journal of Catalysis, 37 (1975) 449-461.
[3] C.H. Bartholomew, R.J. Farrauto, Hydrogen production and synthesis gas reactions, Fundamentals of Industrial Catalytic Processes, Second Edition, (2006) 339-486.
[4] B.H. Davis, Fischer– Tropsch Synthesis: Comparison of Performances of Iron and Cobalt Catalysts, Industrial & Engineering Chemistry Research, 46 (2007) 8938-8945.
[5] A. Barbier, A. Tuel, I. Arcon, A. Kodre, G.A. Martin, Characterization and catalytic behavior of Co/SiO 2 catalysts: influence of dispersion in the Fischer–Tropsch reaction, Journal of catalysis, 200 (2001) 106-116.
[6] A. Lapidus, A. Krylova, J. Rathousky, A. Zukal, M. Janc˘a, Hydrocarbon synthesis from carbon monoxide and hydrogen on impregnated cobalt catalysts II: Activity of 10% Co/Al2O3 and 10% Co/SiO2 catalysts in Fischer-Tropsch synthesis, Applied Catalysis A: General, 80 (1992) 1-11.
[7] G.W. Huber, C.G. Guymon, T.L. Conrad, B.C. Stephenson, C.H. Bartholomew, Hydrothermal stability of Co/SiO2fischer-tropsch synthesis catalysts, (2001).
[8] H. Li, J. Li, H. Ni, D. Song, Studies on cobalt catalyst supported on silica with different pore size for Fischer–Tropsch synthesis, Catalysis letters, 110 (2006) 71-76.
[9] J. Li, Y. Xu, D. Wu, Y. Sun, Hollow mesoporous silica sphere supported cobalt catalysts for F–T synthesis, Catalysis Today, 148 (2009) 148-152.
[10] A. Saib, M. Claeys, E. Van Steen, Silica supported cobalt Fischer–Tropsch catalysts: effect of pore diameter of support, Catalysis Today, 71 (2002) 395-402.
[11] D. Carta, M.F. Casula, A. Corrias, A. Falqui, D. Loche, G. Mountjoy, P. Wang, Structural and magnetic characterization of Co and Ni silicate hydroxides in bulk and in nanostructures within silica aerogels, Chemistry of Materials, 21 (2009) 945-953.
[12] B.C. Dunn, P. Cole, D. Covington, M.C. Webster, R.J. Pugmire, R.D. Ernst, E.M. Eyring, N. Shah, G.P. Huffman, Silica aerogel supported catalysts for Fischer–Tropsch synthesis, Applied Catalysis A: General, 278 (2005) 233-238.
[13] P. Dutta, B. Dunn, E. Eyring, N. Shah, G. Huffman, A. Manivannan, M. Seehra, Characteristics of Cobalt Nanoneedles in 10% Co/Aerogel Fischer– Tropsch Catalyst, Chemistry of materials, 17 (2005) 5183-5186.
[14] Z. Ma, B.C. Dunn, G.C. Turpin, E.M. Eyring, R.D. Ernst, R.J. Pugmire, Solid state NMR investigation of silica aerogel supported Fischer–Tropsch catalysts, Fuel processing technology, 88 (2007) 29-33.
[15] R. Xie, D. Li, B. Hou, J. Wang, L. Jia, Y. Sun, Silylated Co 3 O 4-m-SiO 2 catalysts for Fischer–Tropsch synthesis, Catalysis Communications, 12 (2011) 589-592.

[16] L. Shi, J. Chen, K. Fang, Y. Sun, CH 3-modified Co/Ru/SiO 2 catalysts and the performances for Fischer–Tropsch synthesis, Fuel, 87 (2008) 521-526.
[17] A. Fridman, Plasma chemistry, Cambridge university press2008.
[18] H.L. Chen, H.M. Lee, S.H. Chen, Y. Chao, M.B. Chang, Review of plasma catalysis on hydrocarbon reforming for hydrogen production—Interaction, integration, and prospects, Applied Catalysis B: Environmental, 85 (2008) 1-9.
[19] J. Van Durme, J. Dewulf, C. Leys, H. Van Langenhove, Combining non-thermal plasma with heterogeneous catalysis in waste gas treatment: A review, Applied Catalysis B: Environmental, 78 (2008) 324-333.
[20] T. Nozaki, K. Okazaki, Non-thermal plasma catalysis of methane: principles, energy efficiency, and applications, Catalysis today, 211 (2013) 29-38.
[21] E.C. Neyts, K. Ostrikov, M.K. Sunkara, A. Bogaerts, Plasma catalysis: synergistic effects at the nanoscale, Chemical reviews, 115 (2015) 13408-13446.
[22] X. Tu, J. Whitehead, Plasma-catalytic dry reforming of methane in an atmospheric dielectric barrier discharge: Understanding the synergistic effect at low temperature, Applied Catalysis B: Environmental, 125 (2012) 439-448.
[23] E.C. Neyts, Plasma-surface interactions in plasma catalysis, Plasma Chemistry and Plasma Processing, 36 (2016) 185-212.
[24] X. Tu, H.J. Gallon, M.V. Twigg, P.A. Gorry, J.C. Whitehead, Dry reforming of methane over a Ni/Al2O3 catalyst in a coaxial dielectric barrier discharge reactor, Journal of Physics D: Applied Physics, 44 (2011) 274007.
[25] B. Patil, Q. Wang, V. Hessel, J. Lang, Plasma N2-fixation: 1900–2014, Catalysis today, 256 (2015) 49-66.
[26] R. Snoeckx, A. Bogaerts, Plasma technology–a novel solution for CO 2 conversion?, Chemical Society Reviews, 46 (2017) 5805-5863.
[27] V. Rohani, S. Iwarere, F. Fabry, D. Mourard, E. Izquierdo, D. Ramjugernath, L. Fulcheri, Experimental study of hydrocarbons synthesis from syngas by a tip–tip electrical discharge at very high pressure, Plasma Chemistry and Plasma Processing, 31 (2011) 663.
[28] S. Iwarere, V. Rohani, D. Ramjugernath, F. Fabry, L. Fulcheri, Hydrocarbons synthesis from syngas by very high pressure plasma, Chemical Engineering Journal, 241 (2014) 1-8.
[29] W.S. Al-Harrasi, K. Zhang, G. Akay, Process intensification in gas-to-liquid reactions: plasma promoted Fischer-Tropsch synthesis for hydrocarbons at low temperatures and ambient pressure, Green Processing and Synthesis, 2 (2013) 479-490.
[30] T. Manley, The electric characteristics of the ozonator discharge, Transactions of the electrochemical society, 84 (1943) 83-96.
[31] Y. Wang, M. Noguchi, Y. Takahashi, Y. Ohtsuka, Synthesis of SBA-15 with different pore sizes and the utilization as supports of high loading of cobalt catalysts, Catalysis Today, 68 (2001) 3-9.
[32] D. Yin, W. Li, W. Yang, H. Xiang, Y. Sun, B. Zhong, S. Peng, Mesoporous HMS molecular sieves supported cobalt catalysts for Fischer–Tropsch synthesis, Microporous and mesoporous materials, 47 (2001) 15-24.
[33] V. Jiménez, J. Espinós, A. González‐Elipe, Control of the stoichiometry in the deposition of cobalt oxides on SiO2, Surface and interface analysis, 26 (1998) 62-71.
[34] H. Ming, B.G. Baker, Characterization of cobalt Fischer-Tropsch catalysts I. Unpromoted cobalt-silica gel catalysts, Applied Catalysis A: General, 123 (1995) 23-36.

[35] J. Chai, J. Pan, S. Wang, C. Huan, G. Lau, Y. Zheng, S. Xu, Thermal behaviour of ultra-thin Co overlayers on rutile TiO 2 (100) surface, Surface science, 589 (2005) 32-41.
[36] T. Matsuzaki, K. Takeuchi, T. Hanaoka, H. Arakawa, Y. Sugi, Hydrogenation of carbon monoxide over highly dispersed cobalt catalysts derived from cobalt (II) acetate, Catalysis today, 28 (1996) 251-259.
[37] I. Puskas, T.H. Fleisch, J.B. Hall, B.L. Meyers, R.T. Roginski, Metal-support interactions in precipitated, magnesium-promoted cobaltsilica catalysts, Journal of Catalysis, 134 (1992) 615-628.
[38] T. Motohashi, Y. Katsumata, T. Ono, R. Kanno, M. Karppinen, H. Yamauchi, Synthesis and Properties of CoO2, the x= 0 End Member of the Li x CoO2 and Na x CoO2 Systems, Chemistry of Materials, 19 (2007) 5063-5066.
[39] V. Volchenok, N. Egorov, V. Komarov, S. Kupriyanov, V. Ochkin, N. Sobolev, E. Truvacheev, Chemical composition of the plasma in a CO laser at room temperature, Sov. Phys.-Tech. Phys.(Engl. Transl.);(United States), 21 (1976).
[40] V.D. Rusanov, A.A. Fridman, The physics of a chemically active plasma, Moscow Izdatel Nauka, (1984).
[41] J.A. Gardella Jr, S.A. Ferguson, R.L. Chin, $\pi^* \leftarrow \pi$ shakeup satellites for the analysis of structure and bonding in aromatic polymers by X-ray photoelectron spectroscopy, Applied spectroscopy, 40 (1986) 224-232.
[42] G. Beamson, D. Clark, N. Hayes, D.S. Law, Effect of crystallinity on the XPS spectrum of poly (ethylene terephthalate), Surface Science Spectra, 3 (1994) 357-365.
[43] K. Im-orb, A. Arpornwichanop, Techno-environmental analysis of the biomass gasification and Fischer-Tropsch integrated process for the co-production of bio-fuel and power, Energy, 112 (2016) 121-132.


Gas/Liquid
product
syngas